LETTERS
PUBLISHED ONLINE: 4 JULY 2016 | DOI: 10.1038/NGEO2751
nature geoscience

Antarctic sea-ice expansion between 2000 and 2014 driven by tropical Pacific decadal climate variability

Gerald A. Meehl[1]*, Julie M. Arblaster[1,2], Cecilia M. Bitz[3], Christine T. Y. Chung[4] and Haiyan Teng[1]

Antarctic sea-ice extent has been slowly increasing in the satellite record that began in 1979[1,2]. Since the late 1990s, the increase has accelerated, but the average of all climate models shows a decline[3]. Meanwhile, the Interdecadal Pacific Oscillation, an internally generated mode of climate variability[4], transitioned from positive to negative[5], with an average cooling of tropical Pacific sea surface temperatures[5], a slowdown of the global warming trend[6–8] and a deepening of the Amundsen Sea Low near Antarctica[1,9–12] that has contributed to regional circulation changes in the Ross Sea region and expansion of sea ice[10]. Here we show that the negative phase of the Interdecadal Pacific Oscillation in global coupled climate models is characterized by anomalies similar to the observed sea-level pressure and near-surface 850 hPa wind changes near Antarctica since 2000 that are conducive to expanding Antarctic sea-ice extent, particularly in the Ross Sea region in all seasons, involving a deepening of the Amundsen Sea Low. These atmospheric circulation changes are shown to be mainly driven by precipitation and convective heating anomalies related to the Interdecadal Pacific Oscillation in the equatorial eastern Pacific, with additional contributions from convective heating anomalies in the South Pacific convergence zone and tropical Atlantic regions.

The observed increase of annual mean Antarctic sea-ice extent from 2000–2014 (linear trend of $+0.57 \pm 0.33 \times 10^6$ km^2 decade^{-1}, error bars are 5–95% confidence intervals, see Methods) was nearly a factor of five larger than the increase from 1979–1999 (linear trend of $+0.12 \pm 0.11 \times 10^6$ km^2 decade^{-1}). Observed seasonal Antarctic-average sea-ice extent trends before the Interdecadal Pacific Oscillation (IPO) transition to negative in the late 1990s[13] (Fig. 1a and Supplementary Fig. 1) for the 1979–1999 period (Fig. 1b) range from slight decreases during December–February (DJF; $-0.04 \pm 0.33 \times 10^6$ km^2 decade^{-1}) to small increases in the other seasons of around $+0.2 \times 10^6$ km^2 decade^{-1}. Only the March–May (MAM) trend ($+0.25 \pm 0.25 \times 10^6$ km^2 decade^{-1}) is marginally statistically significant. The Coupled Model Intercomparison Project Phase 5 (CMIP5) multi-model ensemble mean trends for 1979–1999 show statistically significant decreases in all seasons with larger decreasing trends in the cold seasons of July–August (JJA) and September–November (SON) of roughly -0.40×10^6 km^2 decade^{-1} (Fig. 1d).

The observed trends after the IPO transition to negative in the late 1990s (2000–2014) (Fig. 1a) show significantly larger increasing sea-ice concentration trends in all seasons (values greater than $+0.50 \times 10^6$ km^2 decade^{-1}, Fig. 1c). All but MAM are statistically significant and over a factor of four larger than the trends before the IPO transition to negative in the late 1990s (Fig. 1b) for all seasons (except in MAM where there is a factor of two increase). The largest signals with the smallest error bars are in the cold seasons of JJA and SON.

There are ten CMIP5 historical climate model simulations (out of 262) that produce an early-2000s slowdown in the rate of global surface temperature increase with an average negative phase of the IPO through a fortuitous alignment of the randomly generated internal decadal variability in the models happening to match the randomly generated internal variability in the observed system[13]. Those model ensemble members show statistically significant increases in Antarctic sea-ice extent in all seasons, with largest increases in the cold seasons of JJA and SON of greater than $+1.0 \times 10^6$ km^2 decade^{-1} (Fig. 1e). The multi-model average of all other ensemble members shows ongoing decreases (Fig. 1d). About a quarter of all the CMIP5 ensemble members show some positive Antarctic sea-ice trends for the 2000–2014 period (Supplementary Fig. 2), but the amplitude of the trends is roughly half that of the trends associated with the ensemble members with negative IPO (Fig. 1e).

Anomalous positive v-component 850 hPa winds (blowing from the south) are strongly connected with increasing Antarctic sea-ice extent. To quantify this connection, the numbers of grid points in the observations with sea-ice extent increases greater than 10% and the number of those grid points with anomalous positive v-component 850 hPa winds are shown for the pre-1999 and post-2000 epochs (Fig. 1f). There is roughly a factor of two to five more grid points with increasing sea-ice extent in the post-2000 period for all seasons compared with the pre-1999 period. Grid points with positive v-component winds range from about 20% more in SON to over a factor of three greater in JJA for the post-2000 period. Zonal mean v-component winds in the pre-1999 and post-2000 epochs (Fig. 1g) also show the latter period having stronger northward winds than the former. This physically ties positive v-component 850 hPa winds to grid points with increasing sea-ice extent as noted in previous studies.

There is evidence that internal decadal variability of the climate system could be responsible for trends of Antarctic sea ice, such as those recently observed, because such fluctuations have been shown to be close to those arising from internally generated variability in climate models[1,2,14,15]. There are also indications that decadal variability from the tropical Pacific[9,15–17] or tropical Atlantic[18,19] could be playing a role.

While there have been areas of both increasing and decreasing trends of Antarctic sea ice since 2000 (Fig. 2), a deepening of the Amundsen Sea Low (ASL, Supplementary Fig. 1b has

[1]National Center for Atmospheric Research, Boulder, Colorado 80307, USA. [2]Monash University, Melbourne 3008, Australia. [3]University of Washington, Seattle, Washington 98195, USA. [4]Bureau of Meteorology, Melbourne 3001, Australia. *e-mail: meehl@ucar.edu

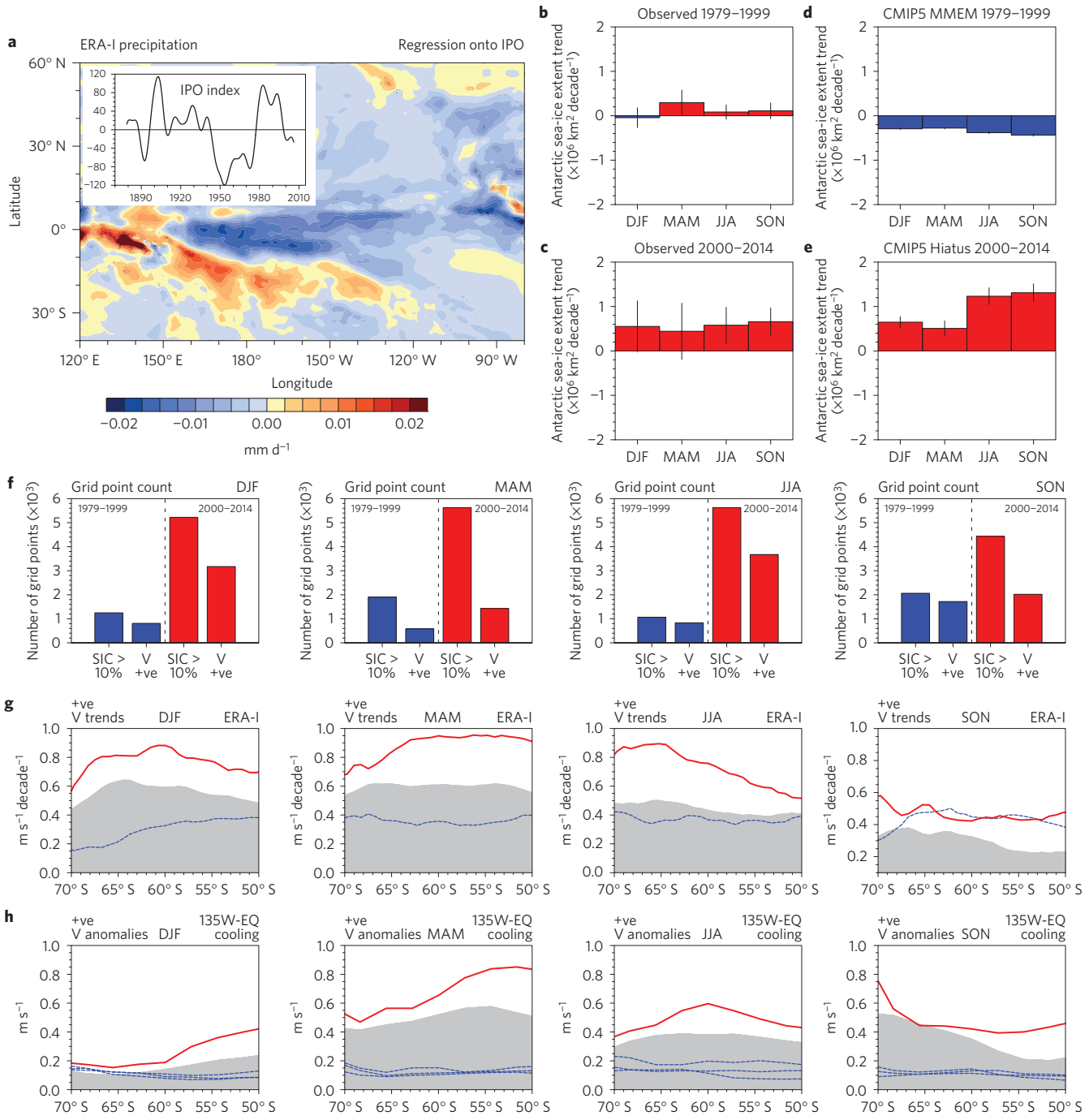

Figure 1 | IPO connection to tropical precipitation, Antarctic sea-ice trends and 850 hPa wind trends. a, Observed precipitation (1979–2014) regressed onto IPO index (inset); sign convention is negative IPO phase. **b**, Antarctic sea-ice extent trends (10^6 km^2 decade^{-1}), 1979–99, with 95% confidence bars. **c**, Same as **b** except for 2000–2014. **d**, Same as **b** except for CMIP5 model averages, 1979–99; MMEM, multi-model ensemble mean. **e**, Same as **d** except for composite trends for ten CMIP5 ensemble members with observed global-averaged surface temperature trend and negative IPO phase[13]. **f**, For each panel, the two bars at the left are the number of grid points, 1979–99 observations, with sea-ice concentrations (SIC) increasing more than 10%, and the number of those grid points with positive ('+ve') 850 hPa v-component winds; two bars at right, the same as those at the left except for the period 2000–2014. **g**, Observed DJF zonal mean positive ('+ve') 850 hPa v-component wind trends (m s^{-1} decade^{-1}), 70° S to 50° S, 2000–2014 (red solid), 1979–1999 (blue dashed), noise estimate (grey shading, one standard deviation of 850 hPa v-component winds at each latitude). **h**, Same as **g** except for positive ('+ve') 850 hPa v-component wind anomalies (m s^{-1}) from the CAM3 model experiment (negative heat source at 135° W, Equator), 30-year average (red solid), three different control run 30-year averages (blue dashed).

Antarctic geographic place names) has been noted to be a major contributor to the average increase in Antarctic sea-ice extent[1,10,20–23]. Previous studies have shown that teleconnections from both tropical Pacific and tropical Atlantic precipitation anomalies, through the agent of convective heating anomalies and an anomalous atmospheric Rossby wave response, can contribute to ASL magnitude[18,19,24]. The question remains regarding what set of processes and mechanisms and from which regions are primarily responsible for the accelerated expansion of Antarctic sea-ice extent after 2000.

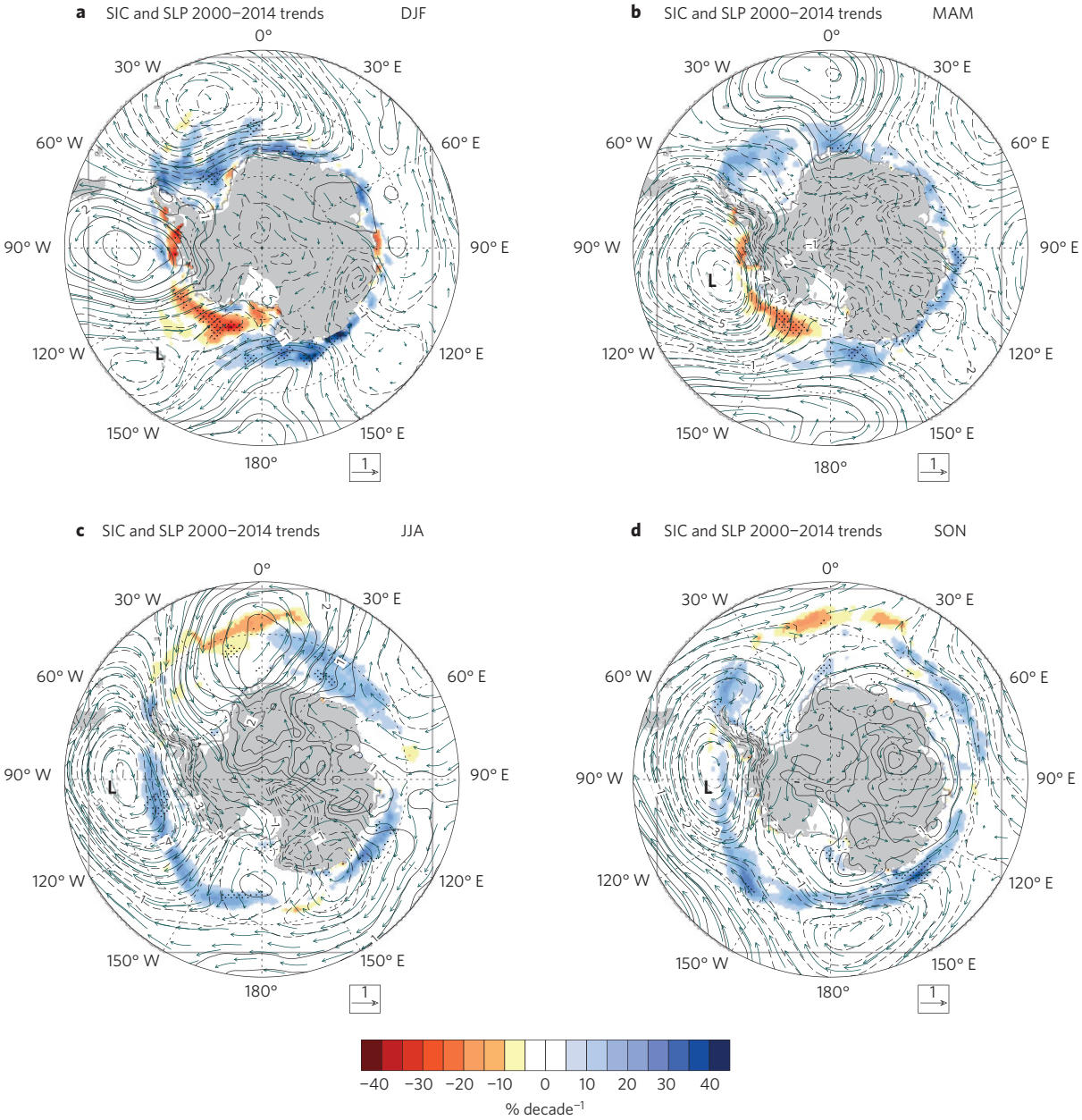

Figure 2 | Observed trends of SLP, sea-ice concentration and 850 hPa winds. a–d, For the era of negative IPO, 2000–2014, sea-ice concentration (SIC) (trends greater than 2.5% decade^{-1} are plotted as colour shading, values significant at the 5% level are stippled), SLP (hPa decade^{-1}) and 850 hPa wind trends (scaling vector at lower right in each panel, m s^{-1} decade^{-1}) for DJF (**a**), MAM (**b**), JJA (**c**) and SON (**d**). Negative values indicating a deepening of the ASL are denoted by 'L'. (Statistical significance of the SLP trends is generally at the 5% level in most of the negative maxima, with values shown in Supplementary Fig. 7.)

A regression analysis of area-averaged sea-level pressure (SLP) in the ASL region onto observed global precipitation shows negative regression values for precipitation in the equatorial eastern Pacific that are at least a factor of four larger than positive values in the equatorial Atlantic for a deepened ASL (Supplementary Fig. 3, also showing negative values in the ASL region for SLP regressed on to the IPO index in Supplementary Fig. 1g). There also are observed positive precipitation regression values (with deepened ASL) in the South Pacific convergence zone (SPCZ) region of the tropical southwest Pacific that are statistically significant in all seasons but JJA (Supplementary Fig. 3). These values are smaller in magnitude by at least a factor of three compared with the equatorial eastern Pacific. This demonstrates that negative equatorial eastern Pacific precipitation anomalies (and consequent negative convective heating anomalies) associated with the negative phase of the IPO after 2000 are more dominant than other tropical Pacific and Atlantic regions in driving negative SLP anomalies in the ASL and consequent increasing sea-ice extent in all seasons. A multiple linear regression analysis confirms this result in showing the dominant role of sea surface temperature (SST), precipitation and convective heating anomalies for a sample area in the equatorial eastern Pacific (Supplementary Information).

After the IPO transition to negative in 1999, teleconnection patterns in an atmospheric model run with a negative convective heating anomaly associated with the negative SST anomalies in the equatorial eastern Pacific with negative IPO (Fig. 3) (see Methods) show comparable patterns to the observed SLP trends, with negative SLP anomalies in the region of the ASL (comparing Figs 2 and 3).

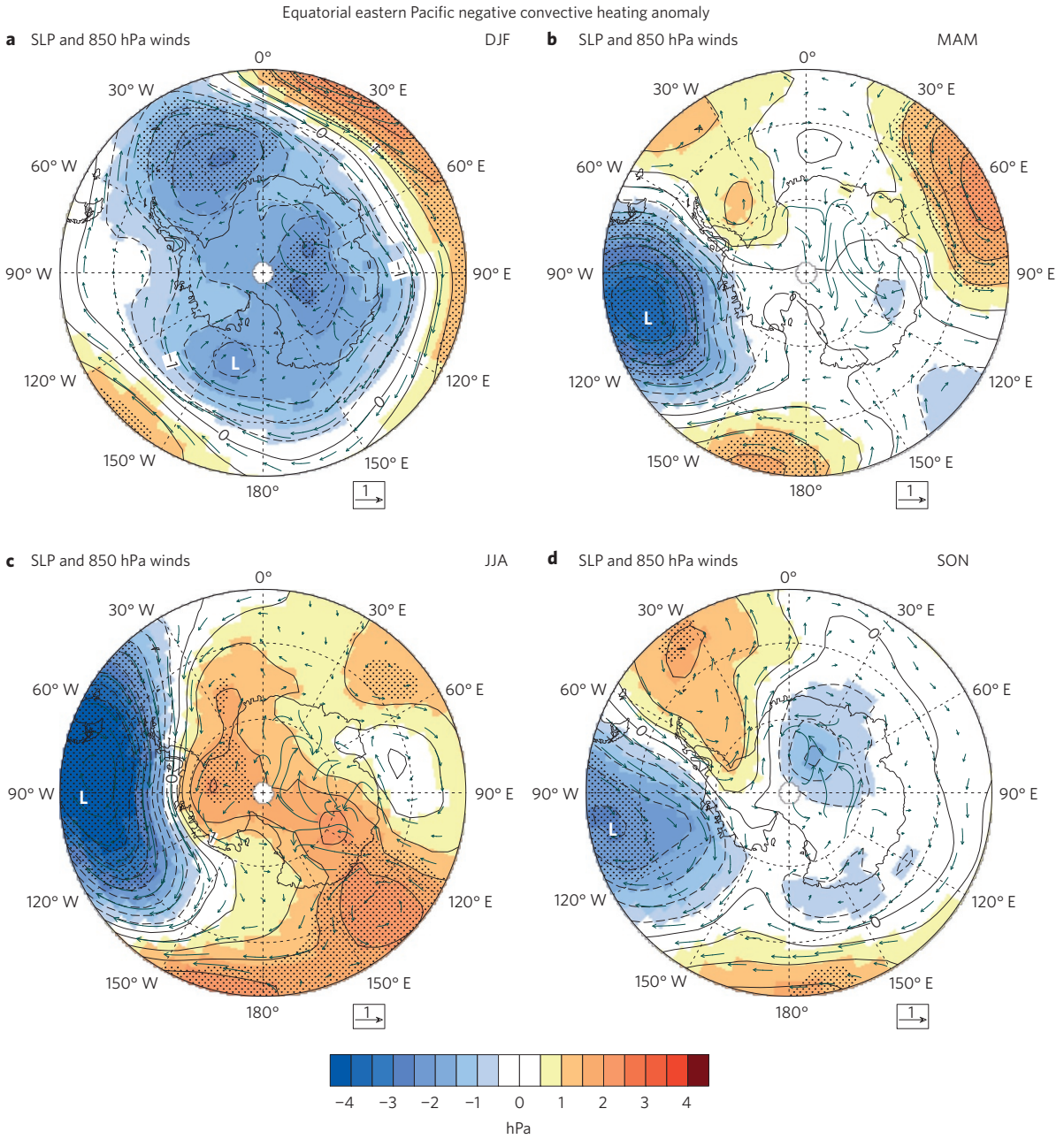

Figure 3 | SLP and 850 hPa wind anomalies for the eastern equatorial Pacific negative heating experiment at 135° W, Equator. Negative SLP anomalies (hPa) shaded blue; positive orange; stippling indicates significance at the 5% level; scaling vector for 850 hPa winds (m s^{-1}) at lower right of each panel. **a**–**d**, Negative values indicating a deepening of the ASL are denoted by 'L', for DJF (**a**), MAM (**b**), JJA (**c**) and SON (**d**).

These SLP anomalies also are consistent with northward component 850 hPa winds (Fig. 1h) and observed sea-ice increases in the Ross Sea sector (Fig. 2).

Forcing from the tropical Atlantic, driven by positive convective heating there associated with positive SST trends (see Extended Data Fig. 6c in ref. 18), contributes to a deeper ASL in MAM (Supplementary Fig. 5b) and increases of Antarctic sea ice in MAM (Fig. 2b) acting in concert with the forcing from the eastern equatorial Pacific that also produces negative SLP anomalies in the ASL region (Fig. 3b). However, the observed negative SLP trends in the ASL region in the other three seasons (Fig. 2a,c,d) have a greater correspondence with similar SLP anomalies produced by a negative convective heating anomaly in the equatorial eastern Pacific (Fig. 3a,c,d). For DJF there is little contribution to observed negative SLP anomalies in the ASL region (Fig. 2a) from convective heating anomalies in the tropical Atlantic (Supplementary Fig. 5a), but there is a closer resemblance to the experiment with the negative convective heating anomaly in the equatorial eastern Pacific (Fig. 3a) with more zonal SLP anomalies[25] and a low-amplitude negative SLP anomaly centre near the Ross Sea that provides northward 850 hPa winds to contribute to the observed increases of sea ice there (Fig. 2a). For MAM, both tropical Pacific and tropical Atlantic convective heating anomalies contribute to a deepened ASL (Fig. 3b and Supplementary Fig. 5b), although the Pacific contribution in the ASL region is nearly two times the magnitude of that from the Atlantic.

For the positive phase of the IPO before 1999 (Fig. 1a), the one season when there were significant increases of Antarctic sea ice was MAM (Fig. 1c), with areas of largest statistically significant increase in the Ross Sea sector (Supplementary Fig. 4a). The tropical

Atlantic positive convective heating anomaly experiment shows an SLP anomaly pattern with a deepened ASL and 850 hPa winds blowing to the north in the Ross Sea region (Supplementary Fig. 5b) would act to drive sea ice equatorward and expand sea-ice extent, with cold air advected from the south to contribute to sea-ice expansion in that season[1] (Supplementary Fig. 4). The equatorial eastern Pacific teleconnection for the positive phase of the IPO at this time would produce positive SLP anomalies in the ASL region (opposite in sign to those for a negative convective heating anomaly in Fig. 3b), and thus would act in the opposite sense. The warming trend of tropical Atlantic SSTs slowed down after 2000 (see Extended Data Fig. 6c in ref. 18), indicating that the forcing from the tropical Atlantic after 2000 could have been less of a factor than that before 2000. After 2000, ongoing Indian Ocean warming most likely produced record Pacific trade winds and stronger negative IPO after 2000[8,26]. Thus, the forcing from the tropical Pacific with positive IPO is very likely less than the forcing from the tropical Atlantic before 1999, and most of the increase of Antarctic sea-ice increase in MAM from 1979–99 can be traced to forcing from the tropical Atlantic during that time period.

Previous studies have noted the connection between positive SPCZ spring (SON) precipitation anomalies and a deepening of the ASL, and are consistent with the negative phase of the IPO[10] (Fig. 2c). It was noted above that SPCZ precipitation (and convective heating anomalies) contributes to ASL SLP anomalies, although with a proportionately smaller contribution than from the equatorial eastern Pacific. SLP anomalies with a specified positive convective heating anomaly at 170° E, 20° S indeed show negative SLP anomalies in the ASL region in SON (Supplementary Fig. 6d). However, there is little correspondence to the correct location of the deepened ASL from observations (Fig. 2a–c) in the other three seasons for the SPCZ forcing (Supplementary Fig. 6a–c). Therefore, SPCZ convective heating anomalies do contribute to the observed ASL anomalies and are consistent with the negative phase of the IPO, but the equatorial eastern Pacific is the dominant forcing for the observed ASL anomalies, and consequent sea-ice expansion, from 2000–2014 in all seasons.

Another factor that could have affected winds and sea-ice extent is the positive Southern Annular Mode trend associated with stratospheric ozone decrease[27]. By calculating the SLP trends from single-forcing ozone-only CMIP5 climate model simulations and subtracting those forced trends from the observations, the trend patterns in Fig. 2 show little change. This is consistent with studies suggesting that the Southern Annular Mode and ozone trends have not contributed significantly to the observed sea-ice increases[28,29], and that internally generated decadal-timescale variability from the IPO can dominate regional atmospheric circulation and sea-ice trends in the Antarctic region on those timescales.

Methods

Methods, including statements of data availability and any associated accession codes and references, are available in the online version of this paper.

Received 26 February 2016; accepted 27 May 2016; published online 4 July 2016

References

1. Turner, J., Hosking, J. S., Marshall, G. J., Phillips, T. & Bracegirdle, T. J. Antarctic sea ice increase consistent with intrinsic variability of the Amundsen Sea Low. *Clim. Dynam.* **46,** 2391–2402 (2015).
2. Gagne, M. E., Gillett, N. P. & Fyfe, J. C. Observed and simulated changes in Antarctic sea ice extent over the past 50 years. *Geophys. Res. Lett.* **42,** 90–95 (2015).
3. Collins, M. *et al*. in *Climate Change 2013: The Physical Science Basis* (eds Stocker, T. F. *et al*.) 1029–1136 (Cambridge Univ. Press, 2013).
4. Power, S. Interdecadal modulation of the impact of ENSO on Australia. *Clim. Dynam.* **15,** 319–324 (1999).
5. Lee, T. & McPhaden, M. J. Decadal phase change in large-scale sea level and winds in the Indo-Pacific region at the end of the 20th century. *Geophys. Res. Lett.* **35,** L01605 (2008).
6. Meehl, G. A. *et al*. Model-based evidence of deep-ocean heat uptake during surface-temperature hiatus periods. *Nature Clim. Change* **1,** 360–364 (2011).
7. Kosaka, Y. & Xie, S.-P. Recent global-warming hiatus tied to equatorial Pacific surface cooling. *Nature* **501,** 403–407 (2013).
8. England, M. H. *et al*. Slowdown of surface greenhouse warming due to recent Pacific trade wind acceleration. *Nature Clim. Change* **4,** 222–227 (2014).
9. Clem, K. R. & Fogt, R. L. South Pacific circulation changes and their connection to the tropics and regional Antarctic warming in austral spring, 1979–2012. *J. Geophys. Res.* **120,** 2773–2792 (2015).
10. Clem, K. R. & Renwick, J. A. Austral spring Southern Hemisphere circulation and temperature changes and links to the SPCZ. *J. Clim.* **28,** 7371–7384 (2015).
11. Turner, J., Phillips, T., Hosking, J. S., Marshall, G. J. & Orr, A. The Amundsen Sea low. *Int. J. Climatol.* **33,** 1818–1829 (2013).
12. Fogt, R. L., Wovrosh, A. J., Langen, R. A. & Simmonds, I. The characteristic variability and connection to the underlying synoptic activity of the Amundsen Bellingshausen Seas low. *J. Geophys. Res.* **117,** D07111 (2012).
13. Meehl, G. A., Teng, H. & Arblaster, J. M. Climate model simulations of the observed early-2000s hiatus of global warming. *Nature Clim. Change* **4,** 898–902 (2014).
14. Polvani, L. M. & Smith, K. L. Can natural variability explain observed Antarctic sea ice trends? New modeling evidence from CMIP5. *Geophys. Res. Lett.* **40,** 3195–3199 (2013).
15. Hobbs, W. R., Bindoff, N. L. & Raphael, M. N. New perspectives on observed and simulated Antarctic sea ice extent trends using optimal fingerprinting techniques. *J. Clim.* **28,** 1543–1560 (2015).
16. Ciasto, L. M., Simpkins, G. R. & England, M. H. Teleconnections between tropical Pacific SST anomalies and extratropical Southern Hemisphere climate. *J. Clim.* **28,** 56–65 (2015).
17. Ding, Q. & Steig, E. J. Temperature change on the Antarctic Peninsula linked to tropical Pacific. *J. Clim.* **26,** 7570–7585 (2013).
18. Simpkins, G. R., McGregor, S., Taschetto, A. S., Ciasto, L. M. & England, M. H. Tropical connections to climatic change in the extratropical Southern Hemisphere: the role of Atlantic SST trends. *J. Clim.* **27,** 4923–4936 (2014).
19. Li, X., Holland, D. M., Gerber, E. P. & Yoo, C. Impacts of the north and tropical Atlantic Ocean on the Antarctic Peninsula and sea ice. *Nature* **505,** 538–542 (2014).
20. Holland, P. R. & Kwok, R. Wind-driven trends in Antarctic sea-ice drift. *Nature Geosci.* **5,** 872–875 (2012).
21. Hobbs, W. R. & Raphael, M. N. The Pacific zonal asymmetry and its influence on Southern Hemisphere sea ice variability. *Antarct. Sci.* **22,** 559–571 (2010).
22. Hosking, J. S., Orr, A., Marshall, G. J., Turner, J. & Phillips, T. The influence of the Amundsen-Bellingshausen Seas low on the climate of West Antarctica and its representation in coupled climate model simulations. *J. Clim.* **26,** 6633–6648 (2013).
23. Raphael, M. N. *et al*. The Amundsen Sea Low: variability, change, and impact on Antarctic climate. *Bull. Am. Meteorol. Soc.* **97,** 111–121 (2016).
24. Li, X., Holland, D. M., Gerber, E. P. & Yoo, C. Rossby waves mediate impacts of tropical oceans on West Antarctic atmospheric circulation in Austral winter. *J. Clim.* **28,** 8151–8164 (2015).
25. Karoly, D. J. Southern Hemisphere circulation features associated with El Niño-Southern Oscillation events. *J. Clim.* **2,** 1239–1252 (1989).
26. Han, W. *et al*. Indian Ocean sea level change in a warming climate. *Nature Geosci.* **3,** 546–550 (2010).
27. Arblaster, J. M. & Meehl, G. A. Contribution of various external forcings to trends in the Southern Annular Mode. *J. Clim.* **19,** 2896–2905 (2006).
28. Simpkins, G., R,Ciasto, L. M., Thompson, D. W. J. & England, M. H. Seasonal relationships between large-scale climate variability and Antarctic sea ice concentration. *J. Clim.* **25,** 5451–5469 (2012).
29. Sigmond, M. & Fyfe, J. C. The Antarctic sea ice response to the ozone hole in climate models. *J. Clim.* **27,** 1336–1342 (2014).

Acknowledgements

Portions of this study were supported by the Regional and Global Climate Modeling Program (RGCM) of the US Department of Energy's Office of Biological & Environmental Research (BER) Cooperative Agreement no. DE-FC02-97ER62402, and the National Science Foundation. C.M.B. is grateful for funding from the National Science Foundation through grant PLR-1341497. We acknowledge the World Climate Research Programme's Working Group on Coupled Modelling, which is responsible for CMIP, and we thank the climate modelling groups for producing and making available their model output. Parts of this research used resources of the National Energy Research Scientific Computing Center, which is supported by the Office of Science of the US Department of Energy under Contract No. DE-AC02-05CH11231. For CMIP, the US Department of Energy's Program for Climate Model Diagnosis and Intercomparison provides coordinating support and led development of software infrastructure in

partnership with the Global Organization for Earth System Science Portals. The National Center for Atmospheric Research is sponsored by the National Science Foundation.

Author contributions

G.A.M. directed this work with contributions from all authors. G.A.M., J.M.A., C.M.B., C.T.Y.C. and H.T. performed the analyses. All of the authors discussed the results and contributed to writing the manuscript.

Additional information

Supplementary information is available in the online version of the paper. Reprints and permissions information is available online at www.nature.com/reprints. Correspondence and requests for materials should be addressed to G.A.M.

Competing financial interests

The authors declare no competing financial interests.

Methods

The IPO is defined as the second empirical orthogonal function (EOF) of low-pass-filtered observed SSTs for the period 1870–2014 (Supplementary Fig. 1), and the IPO index here is defined as the PC time series of the second EOF (Supplementary Fig. 1 shows EOF2 pattern). The observed precipitation (ERA-Interim; comparable calculation for Global Precipitation Climatology Project (GPCP) precipitation in Supplementary Fig. 1h), 1979–2014, is regressed onto the IPO index in Fig. 1a. The sign convention in Fig. 1a is for the negative phase of the IPO as it appeared after 2000 with negative precipitation anomalies in the equatorial eastern Pacific east of about 160° E, and positive anomalies in the SPCZ in the tropical southwest Pacific (compare with observed precipitation anomalies in Supplementary Fig. 1d,e).

The 5% and 95% confidence intervals for the observed sea-ice trends and single model ensemble members are computed as follows:

$$\sigma^2 = \frac{s[x(t) - x'(t)]^2}{\sum_1^t (t - \bar{t})^2}$$

where the variance (σ^2) is equal to the standard deviation of the anomalies for each year from the linear trend (numerator), divided by the sum of the squares of the individual years minus the average number of years. The confidence intervals are $\pm 1.86 \times$ the square root of the variance.

The comparable calculation for N CMIP5 ensemble members is:

$$\sigma^2 = \frac{\sum_1^N \sigma_N^2}{N}$$

Owing to the complex coupled nature of the processes in the climate system, it is difficult to consider the effect of each process individually. One that can be considered in isolation is the influence of tropical precipitation anomalies on midlatitude atmospheric circulation. Previous studies have used specified SST anomalies to produce consequent precipitation and convective heating anomalies[18,19,24]. However, it is the convective heating anomalies associated with these SST and precipitation anomalies that drive anomalous Rossby wave responses and remote teleconnections. It has been shown that specifying SSTs does not always produce the correct location and/or amplitude of precipitation and consequent convective heating anomalies[30]. Therefore, it is preferable to directly specify convective heating anomalies in an atmospheric model to assess the response of midlatitude teleconnections. To quantify these possible midlatitude teleconnections between the precipitation and consequent convective heating anomalies produced by tropical SST anomalies associated with the IPO, specified convective heating anomaly experiments with the Community Atmospheric Model version 3 (CAM3) are run here at T42 resolution with climatological monthly varying SSTs[31].

We define local heat sources or sinks in the same positions as the prominent precipitation anomalies that would produce such convective heating anomalies. A positive convective heating anomaly (corresponding to a positive precipitation anomaly) is placed in the CAM3 in the shape of an elongated ellipse in the SPCZ region centred on 20° S, 170° E, where increased precipitation occurs during a hiatus period characterized by the negative phase of the IPO. In another experiment the same positive convective heating anomaly is placed in the tropical Atlantic in a region centred on the Equator, 35° W. This heating has a central value of $+5\,^{\circ}\mathrm{C\,d^{-1}}$ and decreases linearly with distance until it vanishes on an elliptical boundary with a 3,000 km east–west semimajor axis and a 500 km north–south semi-minor axis. In the vertical, the heating has the profile $\sin(\pi p/p_s)$, where p is pressure and p_s is surface pressure. This profile is an approximation to the vertical distribution of long-term heating anomalies that tend to occur in this model. The magnitude of the idealized source produces the same depth-averaged heating across the disc as about a $4\,\mathrm{mm\,d^{-1}}$ precipitation anomaly, which is nearly twice the magnitude of the anomalies in the model at those locations (Supplementary Fig. 1d). Thus, the midlatitude response would likely be larger than in the observed system[30]. The experiment was run for 30 years, and results are shown as anomalies from a 100-year control run that uses specified climatologically varying SSTs. A comparable experiment was run with a specified negative convective heating anomaly with the same characteristics as described above except with opposite sign, centred on the Equator, 135° W in the equatorial eastern Pacific. For JJA, the eastern equatorial Pacific contribution to negative SLP anomalies in the ASL region (Fig. 3c) is nearly twice the contribution from the Atlantic (Supplementary Fig. 5c), although both tropical forcing regions are contributing to deepening the ASL. For SON, nearly all of the observed negative ASL anomaly can be attributed to the tropical forcing from the equatorial eastern Pacific (comparing Fig. 3d and Supplementary Fig. 5d).

The largest negative SLP anomalies in JJA from SPCZ forcing (Supplementary Fig. 6c) are shifted westward about 60° of longitude compared with the observations (comparing Supplementary Fig. 6c to Fig. 2c). In MAM, there is actually a positive SLP anomaly in the ASL region from SPCZ forcing (Supplementary Fig. 6b) and thus opposite in sign to the large negative ASL anomaly in observations (Fig. 2b). In DJF, instead of northward component 850 hPa winds in the Ross Sea sector, there are southward anomaly winds in the SPCZ forcing experiment (comparing Supplementary Fig. 6a and Fig. 2a).

The observed acceleration of the increase of annual mean Antarctic sea-ice extent compared to steady decreases of annual Antarctic sea-ice extent in the CMIP5 models of -0.35 and $-0.30 \times 10^6\,\mathrm{km^2\,decade^{-1}}$ in the two epochs, respectively (Supplementary Fig. 1). This acceleration coincided with a transition to the negative phase of the IPO with cooler observed SSTs in the tropical Pacific in the late 1990s[5,6] (Fig. 1a and Supplementary Fig. 1). There also was reduced precipitation over those cooler equatorial Pacific SSTs, and increased precipitation over positive SST anomalies in the SPCZ region in the southwestern tropical Pacific (Fig. 1b and Supplementary Fig. 1).

A multiple linear regression approach is also used to quantify relative contributions from the tropical Pacific compared with the tropical Atlantic in contributing to atmospheric teleconnections near Antarctica. Area-averaged precipitation for the eastern equatorial Pacific (for example, 160° W–170° W, 5° N–5° S), the SPCZ region in the tropical southwestern Pacific (165° E–175° E, 15° S–25° S), and the equatorial Atlantic (30° W–40° W, 5° N–5° S) are regressed on to area-averaged SLP in the ASL region (55° S–65° S, 70° W–130° W) for the season with largest increases of Antarctic sea-ice extent (SON) since 2000[1,9]. The r^2 explained variance values are 25% (equatorial eastern Pacific), 5% (SPCZ) and 16% (equatorial Atlantic) for the 1980–2014 period. All of these quantities have p values that indicate statistical significance exceeding the 5% level. Additional calculations correlating area-averaged precipitation from those three regions with SLP elsewhere indicate that explained variance (the square of the correlation) at some grid points approaches 40% in the ASL region connected to equatorial eastern Pacific precipitation, over 30% in association with SPCZ precipitation, and peak grid point values less than 20% linked to tropical Atlantic precipitation. Thus, equatorial eastern Pacific precipitation associated with the IPO makes a contribution to ASL variance in SON over the 1980–2014 period that is nearly twice as large as that from the tropical Atlantic and five times larger than the SPCZ. This provides further evidence for the dominant role the tropical Pacific plays in deepening the ASL that produces consequent increasing Antarctic sea-ice extent.

Consistent with the notion that the recent negative phase of the IPO was characterized by greater average Antarctic sea-ice extent than the previous positive IPO phase, there are indications that during the previous negative phase of the IPO that extended from the 1940s to the 1970s (Fig. 1a), Antarctic sea-ice extent in the 1960s[2] was also very likely greater than during the positive phase of the IPO, which existed in the early part of the modern satellite era from 1979–1999 (Fig. 1c).

Code availability. The climate model code and the scripts used to generate the plots in this paper are available from the corresponding author on request.

Data availability. The NASA sea-ice data[32] are available at ftp://sidads.colorado.edu/pub/DATASETS/nsidc0051_gsfc_nasateam_seaice/final-gsfc, and ERA-Interim at http://apps.ecmwf.int/datasets for both SLP and 850 hPa winds. The SSTs used to calculate the IPO index are available from ftp://ftp.cgd.ucar.edu/archive/SSTICE. NOAA OI SSTs (Supplementary Fig. 1c) are available from http://www.esrl.noaa.gov/psd/data/gridded/data.noaa.oisst.v2.html. GPCP precipitation data (Supplementary Fig. 1e and h) are available from http://www.esrl.noaa.gov/psd/data/gridded/data.gpcp.html, and CMIP5 output (Fig. 1b–e) from http://cmip-pcmdi.llnl.gov/cmip5/data_portal.html. The CAM3 climate model data are available from the corresponding author on request.

References

30. Trenberth, K. E., Zhang, Y. & Fasullo, J. T. Relationships among top-of-atmosphere radiation and atmospheric state variables in observations and CESM. *J. Geophys. Res.* **120,** 10074–10090 (2015).
31. Meehl, G. A., Arblaster, J. M. & Chung, C. T. Y. Disappearance of southeast U.S. "warming hole" with the late-1990s transition of the Interdecadal Pacific Oscillation. *Geophys. Res. Lett.* **42,** 5564–5570 (2015).
32. Fetterer, F., Knowles, K., Meier, W. & Savoie, M. *Sea Ice Index Updated Daily* (National Snow and Ice Data Center, 2002); http://dx.doi.org/10.7265/N5QJ7F7W